

Microscopic spin orbit analysis for proton+⁹Be scattering

Zakaria M. M. Mahmoud

Physics Department, Faculty Of Science, King Khalid University, Saudi Arabia.

Physics Department, Faculty of Science, New Valley University, Egypt.

e-mail: zamahmoud@kku.edu.sa

Received 27 September 2021; accepted 26 October 2021

We simultaneously reanalyzed the elastic scattering differential cross-sections ($d\sigma/d\Omega$) and the vector analyzing power (A_y) of p+⁹Be system. This analysis was performed using microscopic folded potentials for both the real central and the spin-orbit. For the imaginary central, we used surface Woods-Saxon (WS) potential. We aimed to test the microscopic spin orbit potential based on the M3Y effective nucleon-nucleon interaction for the light system p+⁹Be. The present calculation showed that the microscopic spin orbit potential satisfactorily reproduce A_y above 8 MeV and qualitatively reproduced A_y below 8 MeV. In addition, we found that the calculated real central potentials successfully reproduced the $d\sigma/d\Omega$ for all the considered energies. From the present analysis, we expected that the present microscopic spin orbit potential could reproduce successfully the A_y for p+nucleus as the incident proton energy increases above 10 MeV.

Keywords: Proton+nucleus scattering; p+⁹Be scattering; p+⁹Be analyzing power; microscopic spin orbit potential; folding model.

DOI: <https://doi.org/10.31349/RevMexFis.68.031203>

1. Introduction

Proton-projectile is one of the well-known nuclear probes. Using the proton as a projectile, we could obtain useful information about the nuclear structure and nuclear interaction. As an example, we could obtain information about the radial distribution of proton, neutron, and nuclear matter inside the nucleus. Moreover, from the proton-nucleus scattering, we could test the reliability of any theoretical model for nuclear structure or interaction.

Systematic studies on proton scattering from light weakly bound He, Li, and Be isotopes were carried out at wide energy ranges [1–9]. Polarized proton scattering from nuclei adds another constraint to the scattering problem and reflects various aspects of nuclear structures and reaction mechanisms. For example, Sakaguchi *et al.* [10] used the polarized proton for scattering from ⁶He to find the appropriate structure of this exotic nucleus. Uesaka *et al.* [11], found through analyzing Sakaguchi's *et al.* data that $d\sigma/d\Omega$ favor the existence of ⁶He two neutrons halo at backward angles and that the cluster structure reproduced reasonably well the experimental data. In addition, they referred to the indirect effect of neutrons halo on A_y calculation. Mahmoud *et al.* [12] reanalyzed the $d\sigma/d\Omega$ and A_y for the p+⁶He system in the framework of the optical model potential using microscopically real central and spin orbit (SO) potentials. They used CDM3Y6 energy and density-dependent version of the effective M3Y nucleon-nucleon (NN) interaction [13]. Their SO potential was calculated using the formalism reported in Ref. [13]. They aimed to study the validity of the microscopic SO potential based on CDM3Y6 effective NN interaction. In addition, they aimed to study the structure effect on the scattering observable for p + halo-nuclei system. As expected from these studies, the scattering of polarized protons shows different behavior in exotic nuclei compared to stable ones.

Many theoretical models were conducted to describe nuclear clustering in the ⁹Be [14, 15]. The exotic ⁹Be nucleus attracted attention because of its Borromean structure and its cluster breakup. For four decades, the elastic scattering of protons from ⁹Be at low energies was extensively studied both experimentally and theoretically. Farag *et al.* [16] analyzed proton elastic scattering observables of ^{9,10,11,12}Be at a wide range of energy between 3 and 200 MeV using the optical model. They calculated $d\sigma/d\Omega$ and A_y and reaction cross sections σ_R using single folding (SF) real potential based on the density and iso-spin dependent M3Y effective NN interaction and imaginary part based on the high energy approximation. They used the Thomas form with a radial form for the SO potential based on the real folded potential. They claimed that the SF potential reproduced the scattering observables for energies up to 100 MeV using the non-relativistic Schrödinger equation. For higher energies, they found that the high energy approximation or the eikonal approximation could reproduce the scattering observables better than the optical model of the non-relativistic Schrödinger equation. Meridi [17] analyzed the elastic scattering of protons from ⁹Be nucleus at incident energies up to 1000 MeV/nucleon. He used energy-dependent microscopic optical model potential based on the density- and isospin-dependent M3Y-Paris nucleon-nucleon (NN) interaction for the real and spin-orbit parts. For the imaginary part, he used the NN-scattering amplitude of the high-energy approximation. His microscopic complex spin-orbit was taken within Breiva-Rook approximation [18]. He found that the optical model potential fails to reproduce the differential cross-section data at energies larger than 100 MeV/nucleon. In addition, he found that a good improvement is obtained by including the surface contribution to the imaginary part. Recently, Maridi *et al.* [19] analyzed elastic scattering data for

$p+^9\text{Be}$ at proton incident energy below 30 MeV by using two techniques. Their two techniques lead to similar normalized values for the existing data and consistently validate that low-energy data to be safely used for further theoretical studies.

Bingham *et al.* [20] measured the $p+^9\text{Be}$ scattering differential cross sections at eleven bombarding energies between 5 and 15.1 MeV. Their data cover a wide angular range from 15° to 170° in the center of mass (c.m.) system. These low energy data were found to differ by 15-20% between different measurements [21]. These data [20] were investigated by Keely *et al.* [21] to trace and remove any normalization inconsistencies using a coherent coupled reaction channels (CRC) method. The results of Keely *et al.* [21] motivated Pakou *et al.* [9] to reanalyze the data for this system using the microscopic JLM complex potential. The results of Keely [21] and Pakou [9] support the conclusion of negligible or no compound elastic contribution to the elastic scattering $d\sigma/d\Omega$ at low energies.

The measured data of the elastic scattering A_y in conjunction with available $d\sigma/d\Omega$ of protons by complex nuclei extended the scope of the optical model. The analysis of A_y data is essential and unique in obtaining information about the nuclear SO interaction. The availability of $d\sigma/d\Omega$ data makes the central parts of the optical model well defined where the SO potential has only a small effect upon the calculated $d\sigma/d\Omega$. So, A_y measurements and analysis are required to determine the SO interaction in a systematic way [22].

The results of Refs. [9, 12, 21] motivated us to reanalyze the elastic scattering of the proton from the exotic ^9Be . The aim is to study the applicability of the microscopic SO potential based on the CDM3Y6 effective NN interaction for this system. In addition, we aimed to examine the success of the central SF real potential for analyzing scattering data at the considered low energy.

2. Theoretical formalism

2.1. Central real potential

In the present work, we used the SF model to calculate the $p+^9\text{Be}$ central real potential. This real central potential is calculated through the folding procedure from the following relation,

$$V(E, R) = \int \rho(r) \nu_{NN}(|\mathbf{s}|, \rho, E) d\mathbf{r}, \quad \mathbf{s} = \mathbf{R} - \mathbf{r}. \quad (1)$$

As shown from Eq. (1), the SF model has two essential ingredients: 1) a realistic NN effective interaction and, 2) target point nucleon density distribution. The energy- and density-dependent CDM3Y6 effective NN interaction [23] is used as an effective NN interaction, $\nu_{NN}(|\mathbf{s}|, \rho, E)$. This effective interaction has the following form,

$$\nu_{NN}(|\mathbf{s}|, \rho, E) = g(E)F(\rho) \left[v_{00(01)}^{D(E_x)}(|\mathbf{s}|) + v_{SO}^{0(1)}(|\mathbf{s}|) \right], \quad (2)$$

where the intrinsic energy $g(E)$ and density $F(\rho)$ dependent factors [13] have the following forms,

$$g(E) = 1.0 - 0.0026 \frac{E}{N}, \quad (3)$$

$$F(\rho) = 0.2658 [1 + 3.8033 \exp(-1.4099\rho) - 4.0\rho]. \quad (4)$$

The radial forms of the iso-scalar (isospin $T = 0$) and iso-vector (isospin $T = 1$) components of the central M3Y-Paris interaction [13] have the following Yukawa forms,

$$v_{00(01)}^{D(E_x)}(|\mathbf{s}|) = \sum_{i=1}^3 Y_{00(01)}^{D(E_x)}(i) \frac{\exp(-R_i|\mathbf{s}|)}{R_i|\mathbf{s}|}. \quad (5)$$

Similarly, the SO components are represented in the Yukawa forms as,

$$v_{SO}^T(|\mathbf{s}|) = \sum_{i=1}^3 Y_{SO}^T(i) \frac{\exp(-R_i|\mathbf{s}|)}{R_i|\mathbf{s}|}. \quad (6)$$

The explicit ranges and strengths parameters of these Yukawa forms as given by Khoa *et al.* [13] are presented in Table I. The direct part of the real central folded potential is computed from,

$$V_{0T}^D(E, R) = \int \rho_T(r) v_{0T}^D(|\mathbf{s}|, \rho, E) d^3r. \quad (7)$$

The exchange part of the real central folded potential is computed from,

$$V_{0T}^{EX}(E, R) = \int \rho_T(R, r) v_{0T}^D(|\mathbf{s}|, \rho, E) \times j_0(k(E_{c.m.}, R)|\mathbf{s}|) d\mathbf{r}, \quad (8)$$

$j_0(x)$ is the zero order spherical Bessel function. $\rho_{0,1}(r)$ are the iso-scalar and iso-vector densities, respectively, which are defined as,

TABLE I. Yukawa ranges and strengths of the central and SO components of the M3Y-Paris effective NN interaction.

i	$R_i \text{ fm}^{-1}$	$Y_{00}^D(i) \text{ MeV}$	$Y_{01}^D(i) \text{ MeV}$	$Y_{00}^{Ex}(i) \text{ MeV}$	$Y_{01}^{Ex}(i) \text{ MeV}$	$Y_{SO}^0(i) \text{ MeV}$	$Y_{SO}^1(i) \text{ MeV}$
1	4.0	11061.625	313.625	-1524.25	-4118.0	-5101.0	-1897.0
2	2.5	-2537.5	223.5	-518.75	1054.75	-337.0	-632.0
3	0.7072	0.0	0.0	-7.8474	2.6157	0.0	0.0

$$\rho_0(r) = \rho_p(r) + \rho_n(r), \quad (9)$$

$$\rho_1(r) = \rho_p(r) - \rho_n(r), \quad (10)$$

$$\rho_0(R, r) = \rho_p(R, r) + \rho_n(R, r), \quad (11)$$

$$\rho_1(R, r) = \rho_p(R, r) - \rho_n(R, r), \quad (12)$$

and $k(E, R)$ is the relative momentum, which has the form,

$$k(E, R) = \sqrt{\frac{2M}{\hbar^2} (E_{c.m.} - V(E, R) - V_C(R))}. \quad (13)$$

Here M stands for the reduced nucleon mass, $V_C(R)$ is the Coulomb potential and $V(E, R)$ is the total real folded nuclear potential. The density matrix $\rho_k(R, r)$, ($k = p, n$), is considered using the following approximation,

$$\rho_i(R, r) = \rho \left(\left| R + \frac{\mathbf{s}}{2} \right| \right) j_1 \left(k_f^i \left[\left| R + \frac{\mathbf{s}}{2} \right| s \right] \right), \quad (14)$$

$$j_1(x) = 3 \frac{\sin(x) - x \cos(x)}{x^3}, \quad (15)$$

$k_f^i(r)$ is the Fermi momentum and approximated as,

$$k_f^i(r) = \sqrt{\frac{5}{3\rho_i(r)} \left(\tau_i(r) - \frac{1}{4} \nabla^2 \rho_i(r) \right)}, \quad (16)$$

$\tau_i(r)$ (the kinetic energy density) has the Thomas-Fermi approximation form [16] as,

$$\tau_i(r) = \frac{3(3\pi^2)^{2/3}}{5} [\rho_i(r)]^{5/3} + \frac{|\nabla \rho_i(r)|^2}{36\rho_i(r)} + \frac{\nabla^2 \rho_i(r)}{3}, \quad (17)$$

$i = p, n.$

where p, n stand for proton and neutron, respectively.

2.2. Central SO potential

The formalism described in an earlier report [13] is used to calculate the SO-potential in the present work. According to

this formalism and using the SO component of CDM3Y6 effective NN interaction and the target nuclear matter density the SO potential is computed microscopically as,

$$V_{SO}(E, R) = -\frac{g(E)F(\rho(R))}{2} \left[\Phi_p(E, R) \frac{1}{R} \frac{d\rho_p(R)}{dR} + \Phi_n(E, R) \frac{1}{R} \frac{d\rho_n(R)}{dR} \right], \quad (18)$$

$$\Phi_p(E, R) = \int_0^\infty v_{SO}^1(s) [1 + j_1(k(E, R)s)] s^4 ds, \quad (19)$$

$$\Phi_n(E, R) = \frac{1}{2} \int_0^\infty (v_{SO}^1(s) [1 + j_1\{k(E, R)s\}] + v_{SO}^0(s) [1 - j_1\{k(E, R)s\}]) s^4 ds. \quad (20)$$

For comparison, we used a Thomas form SO potential with radial form factor based on WS or the SF real central potentials, respectively. Thus the SO potentials used in this work are written formally as,

$$V_{SO}(E, R) = \begin{cases} N_{so} V_{SO}(E, R), \\ \left(\frac{\hbar}{m_\pi c} \right)^2 \frac{V_{SO}}{R} \frac{d}{dR} \frac{1}{\left(1 + \exp \left[\frac{\{R - R_{so}\}}{a_{so}} \right] \right)}, \\ (\lambda_\pi)^2 \frac{N_{so}}{R} \frac{d}{dR} V(E, R). \end{cases} \quad (21)$$

$\lambda_\pi = \hbar/m_\pi c$ is the pion wavelength. In this work, the optical potentials based on the microscopic SO potential is denoted as MI-SO, while that based on WS Thomas form is denoted as PH-SO and that based on the central real is denoted as CE-SO. The ⁹Be density is based on the experimental charge density [24] as,

$$\rho_i(r) = \rho_{0i} (1 + \omega r^2) \exp(-\beta r^2). \quad (22)$$

This density form is known as a modified Gaussian and has charge root-mean-square radius $\langle r_{ch}^2 \rangle^{1/2} = 2.519$. The point

TABLE II. Phenomenological optical model fitting parameters for p+⁹Be system at energies between 3 and 15 MeV.

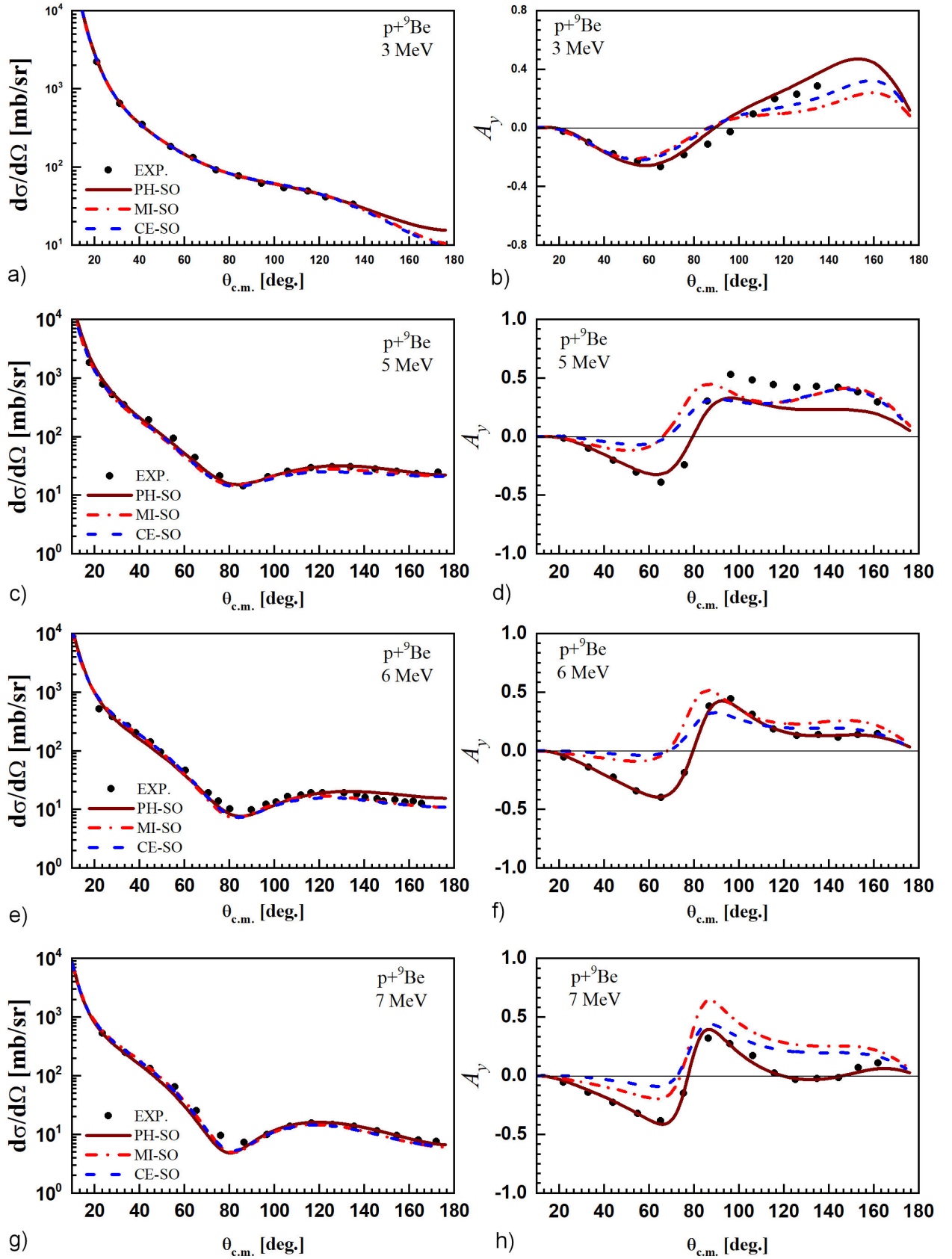
E_p MeV	N_r	W_0 MeV	r_i fm	a_i fm	V_{0so} MeV	r_{so} fm	a_{so} fm
3	1.362	4.365	2.512	0.497	5.719	1.736	0.114
5	1.163	7.218	1.674	0.511	10.403	1.362	0.104
6	1.198	10.732	1.399	0.511	9.635	1.282	0.106
7	1.157	11.484	1.509	0.513	8.471	1.302	0.104
8	1.116	9.926	1.596	0.509	7.252	1.372	0.200
9	1.081	8.788	1.423	0.550	7.225	1.378	0.190
10	1.048	10.080	1.368	0.553	4.564	1.211	0.158
15	1.027	7.496	1.273	0.552	3.833	1.164	0.152

TABLE III. Optical model fitting parameters for $p+{}^9\text{Be}$ system at energies between 3 and 15 MeV.

E_p MeV	Potential	N_r	N_{so}^a	W_0 MeV	r_i fm	a_i fm
3	MI-SO	1.342	1.143	4.220	2.600	0.526
	CE-SO	1.336	0.277	4.035	2.600	0.540
5	MI-SO	1.224	1.555	7.330	1.725	0.511
	CE-SO	1.211	0.328	8.095	1.741	0.511
6	MI-SO	1.135	1.345	11.034	1.607	0.533
	CE-SO	1.112	0.245	12.631	1.589	0.533
7	MI-SO	1.067	1.550	13.140	1.567	0.503
	CE-SO	1.097	0.301	14.392	1.539	0.503
8	MI-SO	1.065	1.242	8.530	1.210	0.545
	CE-SO	1.085	0.255	10.746	1.572	0.505
9	MI-SO	1.070	1.409	7.731	1.164	0.560
	CE-SO	1.169	0.247	14.112	1.117	0.508
10	MI-SO	1.134	1.405	12.946	1.126	0.550
	CE-SO	1.115	0.260	13.565	1.078	0.550
15	MI-SO	1.056	1.200	10.764	1.141	0.540
	CE-SO	1.078	0.275	10.630	1.128	0.556

TABLE IV. Volume integrals for central real, central imaginary and SO potentials.

E_p MeV	Potential	J_r MeV·fm ³	J_i MeV·fm ³	J_{so} MeV·fm ³	σ_R mb
3	PH-SO	855.4	340.5	57.67	992.3
	MI-SO	843.1	373.7	40.26	1027.0
	CE-SO	839.6	367.7	50.90	1033.0
5	PH-SO	719.1	267.4	82.30	659.0
	MI-SO	756.7	287.3	54.24	791.9
	CE-SO	748.5	322.8	58.87	820.2
6	PH-SO	734.5	285.6	71.75	676.9
	MI-SO	696.0	397.8	46.68	818.9
	CE-SO	681.9	446.0	44.02	817.4
7	PH-SO	703.8	352.8	64.07	730.6
	MI-SO	649.0	422.9	53.53	784.6
	CE-SO	667.3	447.7	53.68	779.5
8	PH-SO	673.7	335.2	57.79	749.6
	MI-SO	642.6	189.6	42.68	717.0
	CE-SO	654.7	349.7	45.14	774.4
9	PH-SO	647.2	263.5	57.85	707.0
	MI-SO	640.4	166.5	48.18	671.6
	CE-SO	699.6	250.0	43.39	718.8
10	PH-SO	622.3	283.4	32.11	724.8
	MI-SO	673.2	257.6	47.8	705.4
	CE-SO	662.0	250.5	45.34	709.1
15	PH-SO	586.1	185.0	25.92	572.3
	MI-SO	602.4	213.8	39.85	599.3
	CE-SO	615.0	215.0	46.19	611.0

FIGURE 1. Calculated $d\sigma/d\Omega$ (left panels) and A_y (right panels) for $p+{}^9\text{Be}$ system at energies between 3 and 7 MeV.

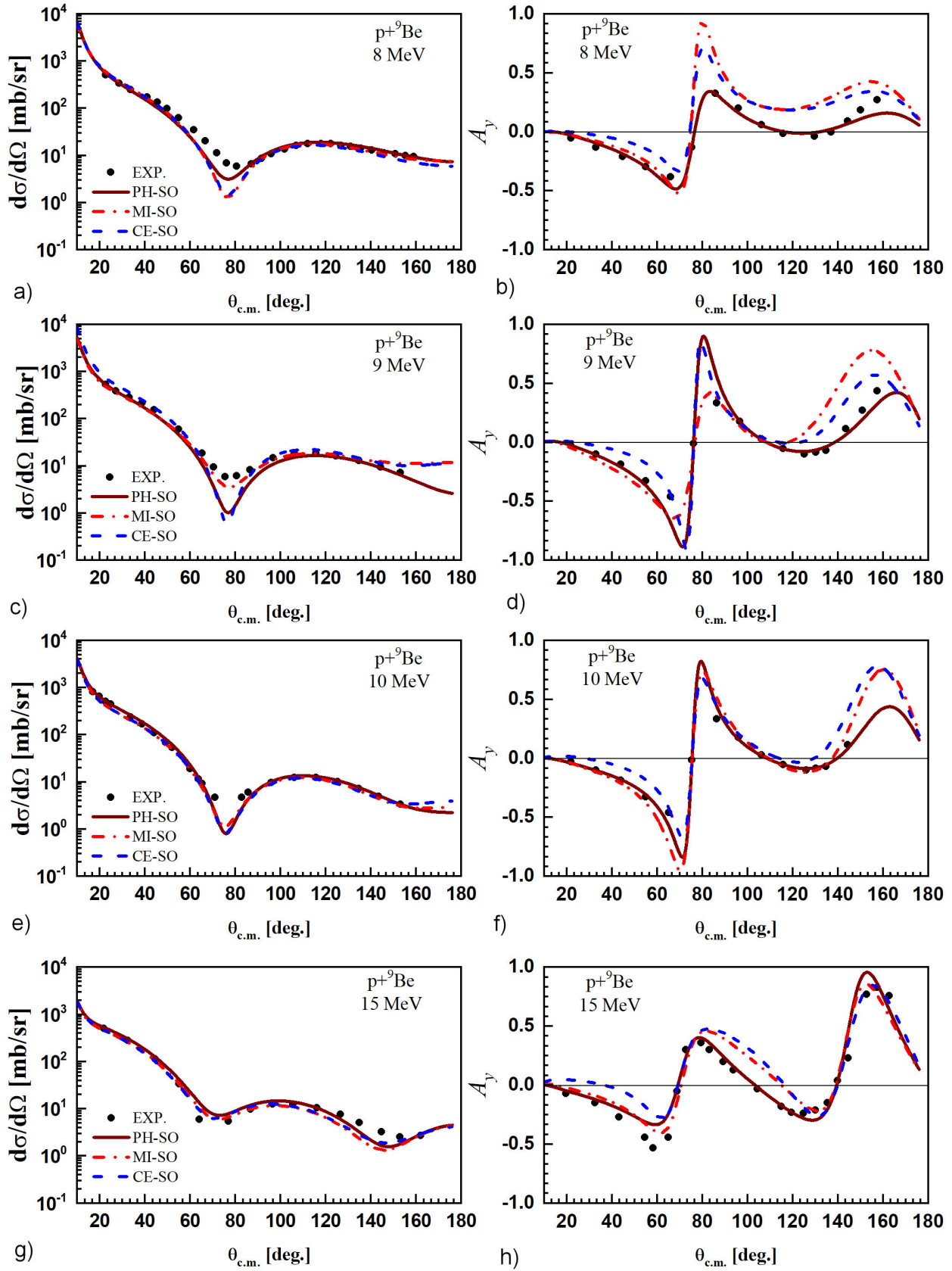


FIGURE 2. Calculated $d\sigma/d\Omega$ (left panels) and A_y (right panels) for $p+{}^9\text{Be}$ system at energies between 8 and 15 MeV.

nucleon density is obtained from this form by unfolding the finite proton size. The obtained density gives $\rho_{0p} = 0.069941$, $\rho_{0n} = 0.0874263$ with point nucleon mean square radius $\langle r_i^2 \rangle = 6.345 - \langle r_{p,ch}^2 \rangle$, where $\langle r_{p,ch}^2 \rangle = 0.76 - 0.11(N/Z)$ [25].

3. Results and discussion

We used the auto-search optical model computer code HERMES [26] to optimize our calculated elastic scattering $d\sigma/d\Omega$ and A_y to the experimental data. The optimization are carried out by minimizing the χ^2 value,

$$\chi^2 = \frac{1}{N} \sum_{i=1}^N \left(\frac{\sigma_{th}(\theta_i) - \sigma_{ex}(\theta_i)}{\Delta\sigma_{ex}(\theta_i)} \right)^2, \quad (23)$$

σ_{th} is the calculated, σ_{ex} is the experimental cross sections at angle θ_i in the c.m. system, $\Delta\sigma_{ex}$ is the experimental error, and N is the number of data points. For the experimental errors, we adopted an average overall value of 10% for all the considered data. Each part of our calculated potential must be multiplied by a re-normalization factor to reproduce the experimental data. Hence, the total nuclear potential $U(E, R)$, which are used to calculate the scattering observables, can be formally written as,

$$U(E, R) = N_r V(E, R) + iW(R) + N_{so} V_{SO}(E, R)(2\vec{L} \cdot \vec{S}), \quad (24)$$

where, \vec{L} is the relative angular momentum and \vec{S} is the spin of the proton. N_r , N_{so} are the re-normalization factors of the central real and SO potentials, respectively.

$$W(R) = 4a_i W_0 \frac{d}{dR} \frac{1}{\left(1 + \exp\left[\frac{\{R-R_i\}}{a_i}\right]\right)},$$

$$R_i = r_i A_T^{1/3}. \quad (25)$$

W_0 , R_i and a_i are the depth and shape parameters of the imaginary potential, respectively. In the optimization procedure, we searched for optimizing N_r , N_{so} and the WS shape parameters for surface imaginary and Thomas form SO potentials, respectively. Our calculated elastic scattering $d\sigma/d\Omega$ and A_y are shown in Figs. 1, 2. The optical model best fit parameters and the corresponding calculated quantities are listed in Tables II-IV.

In Fig. 1 we present the calculated $d\sigma/d\Omega$ (left panels) and A_y (right panels) for p+⁹Be system at energies between 3 and 7 MeV. As shown from this figure, the calculated Ph-, MI- and CE-SO potentials are able to reproduce the experimental $d\sigma/d\Omega$ with equal success. For A_y the MI- and CE-SO potentials failed to reproduce the experimental data successfully but have the same angular distribution pattern. The PH-SO potential is successfully reproduced both the $d\sigma/d\Omega$ and A_y angular distributions for all the considered energies.

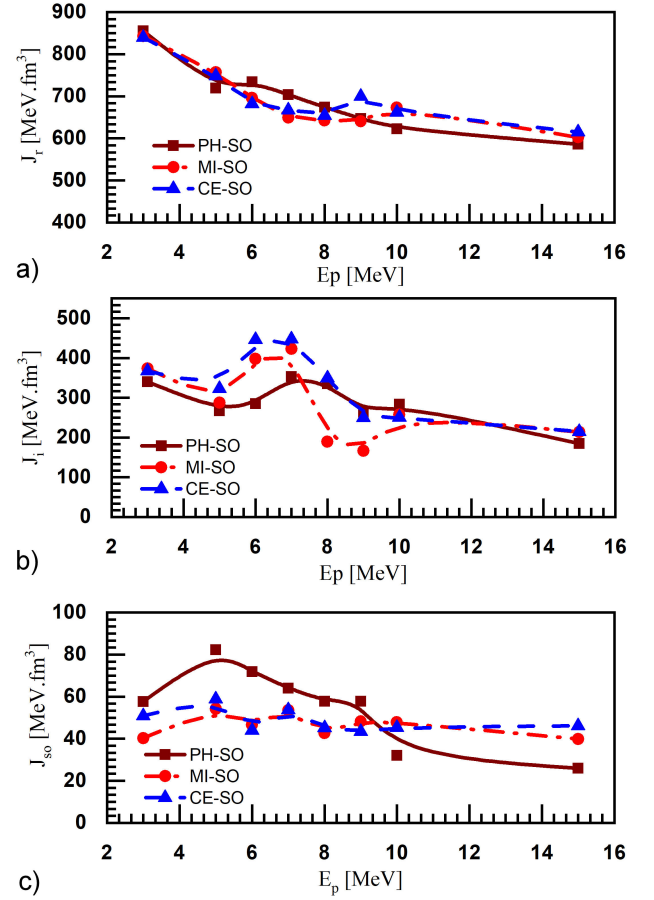


FIGURE 3. The obtained volume integrals J for p+⁹Be system at energies between 3 and 15 MeV.

Moreover, we found that the success of MI-SO and CE-SO potentials are improved in reproducing A_y angular distributions as energy increases.

Our calculated $d\sigma/d\Omega$ (left panels) and A_y (right panels) at energies between 8 and 15 MeV are shown in Fig. 2. As shown in this figure, the MI- and CE-SO potentials reproduced both the $d\sigma/d\Omega$ and A_y reasonably well. The improvement of the calculated A_y started at 8 MeV, where both MI- and CE-SO potentials reproduced the angular distribution successfully at the forward angles up to $\theta \leq 80^\circ$ and overestimated it for larger angles but kept the same angular pattern. As energy increases above 8 MeV, the two potentials reasonably reproduced the A_y over the full considered angular ranges.

The energy dependence of optical model searched parameters, and calculated quantities are shown in Figs. 3, 4. From Fig. 3, we see that the real J_r for the three potentials globally decrease exponential-like with increasing energy. A fine look at this figure shows that the N_r has a small hill at 5, 10, and 9 MeV for Ph-, MI- and CE-SO potentials, respectively. The energy dependence of J_i has a peak at around 6.5 MeV for MI- and CE-SO and at 7 MeV for PH-SO potentials. Moreover, MI-SO potential has a minimum of around 8.5 MeV.

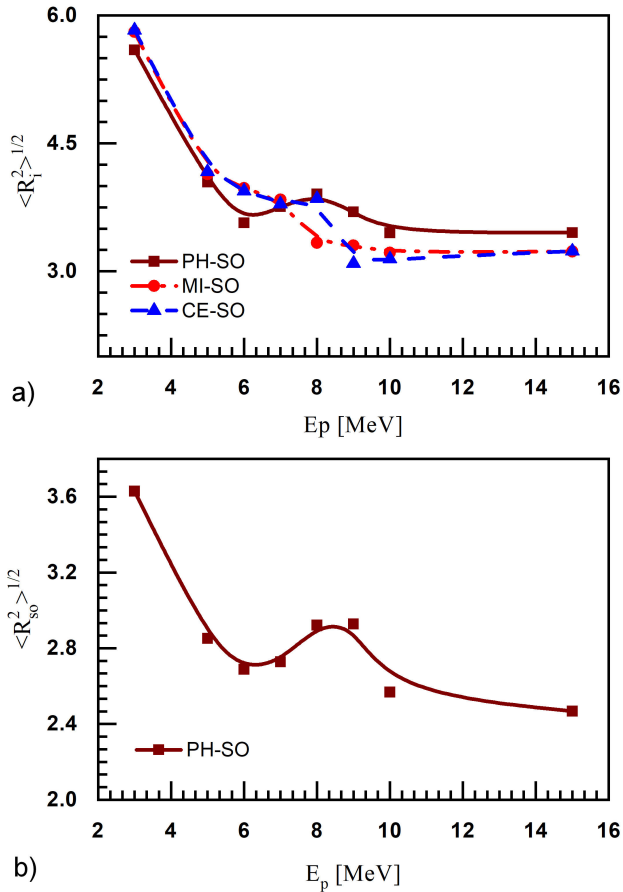


FIGURE 4. The obtained $\langle R_i^2 \rangle^{1/2}$ for p+⁹Be system at energies between 3 and 15 MeV.

The corresponding $\langle R_i^2 \rangle^{1/2}$ (see Fig. 4) has shoulders between 5-8 MeV and 5-9 for MI- CE-SO potentials, respectively. $\langle R_i^2 \rangle^{1/2}$ corresponding to PH-SO potential shows a peak around 8.5 MeV. In general, the $\langle R^2 \rangle^{1/2}$ for the three potentials shows an exponential-like decrease with increasing energy. The SO J_{so} could be approximated with linear relations for MI- and CE-SO potential with a small ripple in the energy interval between 5-9 MeV. For PH-SO potential, J_{so} has a complex energy dependence all over the considered energy range. It is sharply increasing from 3 to 5 MeV and then linearly decreasing from 5–8 MeV. It shows a shoulder from 8 to 9 MeV and then weakly decreases from 10-15 MeV. The $\langle R_{so}^2 \rangle^{1/2}$ for MI-, CE-SO potentials are approximately constant with values 2.660 and 3.197 fm, respectively. The $\langle R_{so}^2 \rangle^{1/2}$ for PH-SO potential is similar in energy behavior to the corresponding $\langle R_i^2 \rangle^{1/2}$ one. That means the $\langle R_{so}^2 \rangle^{1/2}$ for MI-SO potential is less than that of PH-SO potentials for most energies. In contrary, the $\langle R_{so}^2 \rangle^{1/2}$ of CE-SO potential is larger than that of PH-SO potentials for most energies. For compensation, the MI-SO potential has to be re-normalized by more than unity, and CE-SO potential has to be re-normalized by less than unity for all energies to fit the calculated data with the experimental ones.

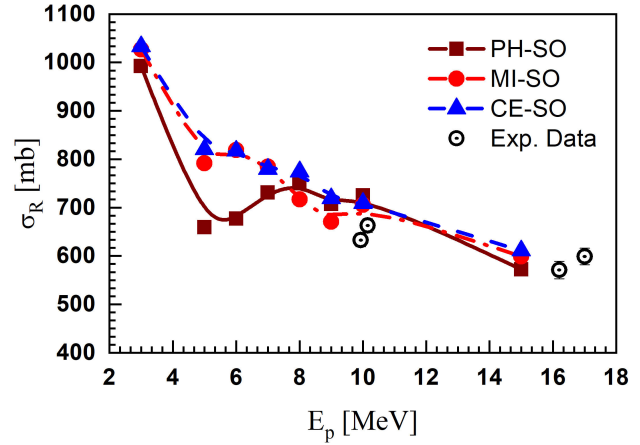


FIGURE 5. Calculated total reaction cross sections σ_R for p+⁹Be system at energies between 3 and 15 MeV.

In Fig. 5, we present the energy dependence of the total reaction cross sections σ_R in comparison with the available experimental data close to the considered energies [27]. As shown in this figure, the calculated σ_R are very close to the experimental ones. Also, the calculated σ_R is very close to the calculated one based on the four body CDCC at energy around 6 MeV [28]. This agreement indicates the success of the present microscopic potential. In addition, we found that the σ_R for MI-, CE-SO potentials has a sharp decrease from 3-5 MeV and then decreases approximately linear with increasing energy from 5-15 MeV. For PH-SO potential, this quantity has a pocket with a minimum of around 5.5 MeV and then has a linear decrease above 8 MeV.

From these energy dependences, we could expect the influence of ⁹Be breakup channel at the energy interval between 5-8 MeV. In addition, we could conclude that the present data are not entirely free from the normalization problem. This conclusion comes from the data analysis at 5 and 6 MeV, where a theory normalization for PH-SO calculation 1.276, 1.123 has to be introduced to reproduce the data, respectively.

4. Conclusion

In the present work, we analyzed the p+⁹Be elastic scattering at 3-15 MeV. Both the differential $d\sigma/d\Omega$ and A_y are analyzed simultaneously in the framework of the optical model. The real part of the optical model potential is computed using the SF procedure. For the SO potential, we adopted microscopic and phenomenological Thomas form methods. For microscopic SF and SO potentials, the CDM3Y6 effective NN interaction is used. In the phenomenological Thomas form method for the SO potential, the radial form factor is chosen in the WS-form (phenomenological form) or in the form of the calculated SF real potential (semi-microscopic form). The optical potential imaginary part is adopted in the conventional surface WS form throughout this analysis.

The optimization of the calculated $d\sigma/d\Omega$ and A_y is done using the spherical optical model code HERMES [26]. We

found that the SF real potential with the different versions of SO potentials can reproduce the $d\sigma/d\Omega$ and the A_y with the phenomenological SO potential for all energies. Also, we found that the microscopic SO potential and the semi-microscopic SO potentials cannot reproduce the A_y at energies below 8 MeV, while they are reasonably and successfully reproduced A_y at energies ≥ 8 MeV. The success of this microscopic SO potential is increased while increasing energy.

In conclusion, we found that the microscopic SO potential is successful in reproducing the analyzing power A_y for the $p+^9\text{Be}$ system contrary to the founding of $p+^6\text{He}$ [12]. The present analysis provides a good application for using the microscopic spin-orbit potential. The success of the mi-

croscopic SO potential motivates us to study the structural effects of ⁹Be on the scattering observable and other calculated quantities. Also, it encourages us to extend it to other nuclei where experimental A_y data exist over a wide energy range.

Acknowledgments

The authors extend their appreciation to the Deanship of Scientific Research at King Khalid University for funding this work through Research Groups Program under grant no. R.G.P.1/78/42.

1. V. K. Lukyanov *et al.*, *Calculations of $^8\text{He} + p$ elastic cross sections using a microscopic optical potential*, Phys. Rev. C **80** (2009) 024609, <https://doi.org/10.1103/PhysRevC.80.024609>.
2. M. Y. H. Farag, E. H. Esmael, and H. M. Maridi, *Microscopic study on proton elastic scattering of helium and lithium isotopes at energy range up to 160 MeV/nucleon.*, EPJ Web of Conferences, **66** (2014) 03025, <https://doi.org/10.1051/epjconf/20146603025>.
3. P. Egelhof, *Nuclear-matter distributions of halo nuclei from elastic proton scattering in inverse kinematics* Eur Phys J A **15**, (2002) 27, <https://doi.org/10.1140/epja/i2001-10219-7>.
4. A. Pakou, *Global description of the $^7\text{Li} + p$ reaction at 5.44 MeV/u in a continuum-discretized coupled-channels approach*, Phys. Rev. C **96** (2017) 034615, <https://doi.org/10.1103/PhysRevC.96.034615>.
5. A. Pakou *et al.*, *Probing the cluster structure of ^7Li via elastic scattering on protons and deuterons in inverse kinematics*, Phys. Rev. C **94** (2016) 014604, <https://doi.org/10.1103/PhysRevC.94.014604>.
6. S. Sakaguchi *et al.*, *Analyzing Power in Elastic Scattering of Polarized Protons from Neutron-rich Helium Isotopes Few-Body Syst.* **54** (2013) 1393, <https://doi.org/10.1007/s00601-013-0617-1>.
7. V. Soukeras *et al.*, *Reexamination of $^6\text{Li} + p$ elastic scattering in inverse kinematics*, Phys. Rev. C **91** (2015) 057601, <https://doi.org/10.1103/PhysRevC.91.057601>.
8. S. P. Weppner, *A nucleon-nucleus optical model for $A \leq 13$ nuclei at 65–75 MeV projectile energy*, J Phys G: Nucl Part Phys **45** (2018) 095102, <https://doi.org/10.1088/1361-6471/aad53d>.
9. A. Pakou *et al.*, *A Microscopic Approach for $p+^9\text{Be}$ at Energies Between 1.7 to 15 MeV/nucleon*, Acta Phys. Polon. **B50** (2019) 1547, <https://doi.org/10.5506/aphyspolb.50.1547>.
10. S. Sakaguchi, *et al.*, *Analyzing Power in Elastic Scattering of ^6He from a Polarized Proton Target at 71 MeV/nucleon*, Phys. Rev. C **84**, (2011) 024604, <https://doi.org/10.1103/PhysRevC.84.024604>.
11. T. Uesaka, *et al.*, *Analyzing power for proton elastic scattering from the neutron-rich ^6He nucleus*, Phys. Rev. C **82** (2010) 021602, <https://doi.org/10.1103/PhysRevC.82.021602>.
12. Zakaria M. M. Mahmoud, and Awad A. Ibraheem, and M. A. Hassanain, *Microscopic spin-orbit potential for $p+^6\text{He}$ elastic scattering*, Int. J. Mod. Phys. E **28** (2019) 1950074, <https://doi.org/10.1142/S0218301319500745>.
13. D. T. Khoa, E. Khan, G. Coló and N. Van Giai, *Folding model analysis of elastic and inelastic proton scattering on sulfur isotopes*, Nucl. Phys. A **706**, (2002) 61, [https://doi.org/10.1016/S0375-9474\(02\)00866-7](https://doi.org/10.1016/S0375-9474(02)00866-7).
14. T. A. D. Brown, *et al.*, *Decay studies for states in ^9Be up to 11 MeV: Insights into the $n+^8\text{Be}$ and $\alpha+^5\text{He}$ cluster structure*, Phys. Rev. C **76**, (2007) 054605, <https://doi.org/10.1103/PhysRevC.76.054605>.
15. P. Papka, *et al.*, *Decay path measurements for the 2.429 MeV state in ^9Be : Implications for the astrophysical $\alpha+\alpha+n$ reaction*, Phys. Rev. C **75** (2007) 045803, <https://doi.org/10.1103/PhysRevC.75.045803>.
16. M. Y. H. Farag, E. H. Esmael, and H. M. Maridi, *Analyzing power for proton- $^{9,10,11,12}\text{Be}$ scattering using an energy-, density-, and isospin-dependent microscopic optical potential*, Phys. Rev. C **90** (2014) 034615, <https://doi.org/10.1103/PhysRevC.90.034615>.
17. H. M. Maridi, *Energy dependence and surface contribution of the folding-model optical potential for nucleon-nucleus scattering at energies up to 1 GeV/nucleon*, Phys. Rev. C **100** (2019) 014613, <https://doi.org/10.1103/PhysRevC.100.014613>.
18. F. A. Brieva and J. R. Rook, *Nucleon-nucleus optical model potential: (III). The spin-orbit component*, Nucl. Phys. A **297** (1978) 206, [https://doi.org/10.1016/0375-9474\(78\)90272-5](https://doi.org/10.1016/0375-9474(78)90272-5).
19. H. M. Maridi, A. Pakou, and K. Rusek, *The $p+^9\text{Be}$ elastic scattering below 30 MeV: Optical model analysis and data normalization*, Int. J. Mod. Phys. E **30**, (2021) 2150024, <https://doi.org/10.1142/S0218301321500245>.

20. F. W. Bingham, M. K. Brussel and J. D. Steben, *Scattering of 5-15 MeV protons from Be⁹*, Nucl. Phys. **55** (1964) 265, [https://doi.org/10.1016/0029-5582\(64\)90145-2](https://doi.org/10.1016/0029-5582(64)90145-2).
21. N. Keeley, *et al.*, *Coherent coupled-reaction-channels analysis of existing and new p + ⁹Be data between 1.7 and 15 MeV/nucleon*, Phys. Rev. C **99** (2019) 014615, <https://doi.org/10.1103/PhysRevC.99.014615>.
22. D. J. Baugh, J. A. R. Griffith and S. Roman, *Polarization of 17.8 MeV protons elastically scattered by nuclei*, Nucl. Phys. B **83** (1966) 481, [https://doi.org/10.1016/0029-5582\(66\)90106-4](https://doi.org/10.1016/0029-5582(66)90106-4).
23. Dao T. Khoa, G. R. Satchler, and W. von Oertzen, *Folding analysis of the elastic ⁶Li + ¹²C scattering: Knock-on exchange effects, energy dependence, and dynamical polarization potential*, Phys. Rev. C **51** (1995) 2069, <https://doi.org/10.1103/PhysRevC.51.2069>.
24. H. De Vries, C. W. De Jager, and C. De Vries, *Nuclear charge and magnetization density distribution parameters from elastic electron scattering*, Atom. Data Nucl. Data Tabl. **36** (1987) 495, [https://doi.org/10.1016/0092-640X\(87\)90013-1](https://doi.org/10.1016/0092-640X(87)90013-1).
25. J. Cook, *DFPOT - A program for the calculation of double folded potentials*, Comput. Phys. Commun. **25** (1982) 125, [https://doi.org/10.1016/0010-4655\(82\)90029-7](https://doi.org/10.1016/0010-4655(82)90029-7).
26. J. Cook, *Hermes - an optical model search program including tensor potentials for projectile spins 0 to 3/2* Comput Phys Commun **31** (1984) 363, [https://doi.org/10.1016/0010-4655\(84\)90020-1](https://doi.org/10.1016/0010-4655(84)90020-1).
27. R. F. Carlson, *Proton-Nucleus Total Reaction Cross Sections and Total Cross Sections Up to 1 GeV*, At. Data. Nucl. Data Tables **63** (1996) 93, <https://doi.org/10.1006/adnd.1996.0010>.
28. V. Soukeras *et al.*, *Global study of ⁹Be + p at 2.72 A MeV*, Phys. Rev. C **102** (2020) 064622, <https://doi.org/10.1103/PhysRevC.102.064622>.